

RESEARCH

Open Access



Structural Behavior of Construction Joints in a Composite Rigid-Frame Bridge

Sanghyeon Cho¹, Jungho Choi¹, Heeyoung Lee² and Wonseok Chung^{1*}

Abstract

Composite rigid-frame bridges with steel girders have excellent structural performance, but behavioral inconsistency appears at the connection between the steel girder and concrete pier. In addition, composite rigid-frame bridges are challenging to construct owing to the need to connect different materials at the pier. Therefore, this study developed and demonstrated a composite rigid-frame bridge with a construction joint and anchors. The structural performance and composite behavior of the proposed construction joint were investigated by evaluating a direct connection between the girder and concrete prior to casting (Joint A), a plain construction joint (Joint B), and a construction joint with anchors (Joint C). Joints B and C exhibited 16.5% and 46.5% higher ultimate capacities, respectively, than did Joint A. Finite element analysis of Joint C was conducted, and its results were verified against the experimental results. Further, parameter analysis was performed to determine the effects of the steel girder strength and anchor diameter. The results indicated that the proposed construction joint with anchors exhibited excellent structural performance and composite behavior.

Keywords Composite rigid-frame bridge, Composite behavior, Construction joint, Anchor, Finite element analysis

1 Introduction

Girder bridges are expensive to construct because they require elastic joints and bearings (Dicleli et al., 2003; Wolde-Tinsae et al., 1988), which also lead to maintenance problems as they undergo rapid aging under load. By contrast, rigid-frame bridges provide excellent economic efficiency, usability, and maintainability because they do not require such readily degradable components. By integrating the load response of the girder and pier using a rigid joint, rigid-frame bridges reduce the magnitude of positive moment at center span by transmitting

not only the vertical and axial loads to the pier but also the bending moment (Feng et al., 2006; Mei, 1999; Zhouhong et al., 2004). However, as the span of a rigid-frame bridge increases, the required concrete girder cross-section increases, as does its self-weight.

Recently, composite rigid-frame bridges were developed to reduce the span weight and improve structural performance by employing steel girders fixed to the concrete pier. This arrangement outperforms other types of bridges in terms of spanning capability and construction cost, owing to its excellent structural performance and reduced cross-section (Adeli & Zhang, 1995; Kwak & Seo, 2000; Xiang et al., 2004). Moreover, composite rigid-frame bridges exhibit excellent maintainability because they do not require joints or bearings (Chung et al., 2013; Lin et al., 2020a, 2020b, 2020c; Nakai et al., 2018; Xie et al., 2018). Xie et al. (2018) found the optimal longitudinal length ratio of steel girders and a composite rigid-frame bridge to be 0.55. Lin et al., (2020a, 2020b, 2020c) conducted three-dimensional finite element analysis (FEA) to analyze the seismic resistance capability of

Journal information: ISSN 1976-0485 / eISSN 2234-1315.

*Correspondence:

Wonseok Chung
wschung@khu.ac.kr

¹ Department of Civil Engineering, College of Engineering, Kyung Hee University, 1732 Deokyoung-Daero, Giheung-Gu, Yongin-Si, Gyeonggi-Do 17104, Republic of Korea

² Department of Civil Engineering, Chosun University, 309-1 Pilmun-Daero, Dong-Gu, Gwangju 61453, Republic of Korea

a 15.6-m-long composite rigid-frame bridge. Chung et al. (2013) analyzed the behavior of a 14.2-m-long composite rigid-frame bridge with vertically pre-tensioned connections between the girders and piers, demonstrating excellent structural performance. Nakai et al. (2018) fabricated a 6.8-m-long steel–concrete composite rigid-frame bridge and analyzed its behavior through load tests; the results showed improved structural performance when steel girders were used instead of concrete girders.

In the design of steel–concrete composite structures such as a composite rigid-frame bridge, the interface between the steel and concrete must be carefully considered, as non-composite behavior may occur as a result of slipping at this interface. The construction joint has therefore been proposed to provide a stronger connection between steel and concrete in general composite structures by casting the final concrete joint after assembling prefabricated steel and concrete segments. Sritharan et al. (2005) observed that a construction joint applied between a steel girder and concrete pier in a composite bridge exhibited excellent seismic performance under cyclic load. Lee et al. (2019) applied a construction joint to connect a precast concrete girder to a steel pier in a 3.1-m-high test unit. The test unit exhibited an ultimate capacity 2.1 times higher than the design load, and the joint itself exhibited excellent structural performance. Zhang et al. (2020) used a construction joint to connect a concrete column to a concrete beam with an embedded steel plate. They observed a 40.6% increase in the ultimate capacity compared with that observed in the case of a monolithic connection formed during concrete pouring.

Steel–concrete composite structures exhibit behavioral inconsistencies at their connections owing to the different properties of their constituent materials. Therefore, it is essential to ensure that steel–concrete joints exhibit adequate structural performance. Recently, several studies utilized anchors to improve the connectivity of steel–concrete composite structures. Ataei et al. (2015) installed anchors to integrate the behaviors of a steel girder and concrete-filled steel tube column, realizing improved integrity and a 1.75 times increase in the ultimate capacity. Ataei et al. (2019) connected steel and concrete using various types of anchors and observed that the behavioral integrity of the steel–concrete composite improved as the anchor diameter increased to realize a two-fold increase in the ultimate capacity of the connection. Nijgh et al. (2019) analyzed the behavior of 14.4-m-long steel–concrete composite beams in which the different materials were connected using anchors, reporting an improvement in the bending stiffness of up to 68% as the anchor spacing decreased. Zhang et al. (2019) fabricated 0.6-m-long steel–concrete composite

beams using various anchor-based connections and observed that, at a constant concrete compressive strength, the ultimate capacity of each anchor improved by up to 1.4 times as the anchor diameter increased.

Studies on construction joints (Lee et al., 2019; Sritharan et al., 2005; Zhang et al., 2020) have reported that they improved the constructability and structural performance of composite structures, including composite rigid-frame bridges. Furthermore, studies that applied anchors to connect the steel and concrete in composite structures (Ataei et al., 2015, 2019; Nijgh et al., 2019; Zhang et al., 2019) indicated an improvement in the composite behavior. Composite rigid-frame bridges can therefore be expected to exhibit excellent structural performance when the connections between the steel girders and concrete piers are improved using a construction joint strengthened with anchors; however, this type of joint has not been considered in previous studies on composite rigid-frame bridges (Chung et al., 2013; Lin et al., 2020a, 2020b, 2020c; Nakai et al., 2018; Xie et al., 2018). Therefore, the present study developed a composite rigid-frame bridge in which the steel girder end segments were connected to the concrete pier using a cast-in-place connection and anchors. To analyze the behavioral integrity and structural performance of the proposed construction joint with anchors in the composite rigid-frame bridge, three 3.35-m-high test units were fabricated and subjected to vertical loading. Subsequently, FEA was conducted, using a model verified against the experimental results, to examine the behavior of the proposed construction joint. The results were used to determine the effects of the connection parameters on joint performance.

2 Proposed Composite Rigid-Frame Bridge

Rigid-frame bridges are prone to issues at their joints owing to the need for tight integration between the superstructure and substructure. Recently, improved structural behavior was realized by applying steel girders to construct composite rigid-frame bridges. However, these bridges can undergo cracking in the pier because of the self-weight of the steel girders, which must be directly fixed to the top of the pier during construction; further, this arrangement makes construction difficult. The composite rigid-frame bridge connection proposed herein was developed to address such joint cracking and constructability issues. Fig. 1a shows a conceptual diagram of the proposed composite rigid-frame bridge at the pier connections, and Fig. 1b shows a conceptual diagram of the proposed construction joint with anchors. In this arrangement, after the concrete pier is constructed with block-outs for the construction joints, a steel girder support is installed on the span side of the joint to share

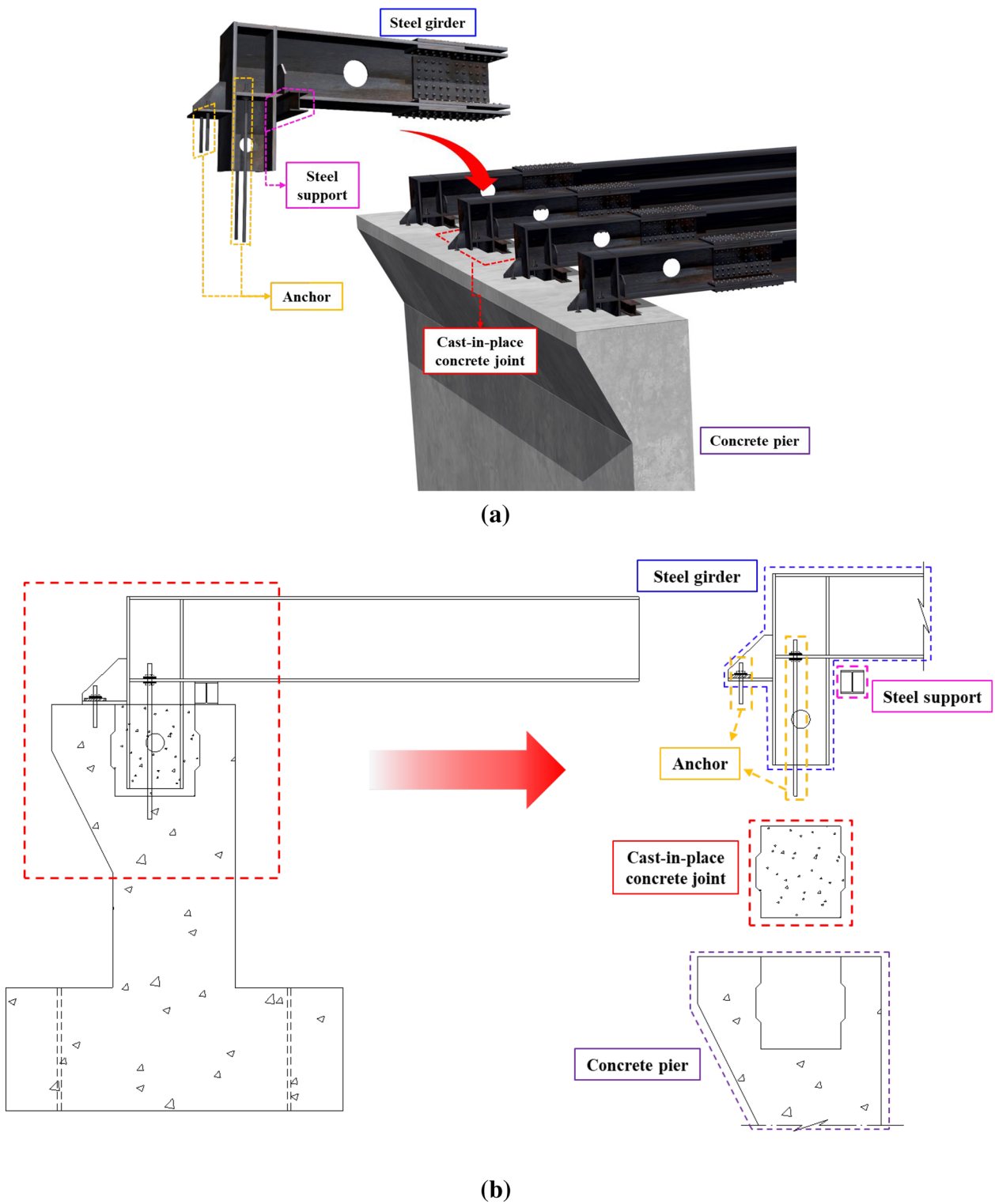


Fig. 1 **a** Three-dimensional rendering of the proposed construction joint in composite rigid-frame bridge and **b** details of the proposed construction joint with anchors

the self-weight of the girders. Then, anchors are installed through the block-out into pre-formed anchor holes in the pier. Subsequently, the entire assembly is cast in concrete by filling in the block-out, and the girders are completed by connecting them at the splices, allowing for the concrete deck on top to be cast shortly thereafter. This joint design provides three notable advantages. First, a shallow span depth is secured by employing steel girders instead of concrete girders, ensuring sufficient overhead clearance beneath the span. Indeed, the proposed composite rigid-frame bridge is advantageous for securing the river cross-section, as a bridge spanning longer than 50 m can be easily installed over small rivers that require sufficient clearance. Second, a high resistance against a negative moment is provided by effectively ensuring the composite behavior of the steel girder and pier at their connection using anchors. This also results in reduced deflection and vibration compared with those observed for typical bridge designs, as well as excellent maintainability, because bearings and elastic joints have been eliminated. Third, the proposed composite rigid-frame bridge can be constructed in less time by simultaneously fabricating the steel girders and pier and then rapidly connecting them to complete the bridge. This ensures that both the positive moment in the completed girder spans and negative moment at the connection to the piers can be effectively accommodated during the construction sequence and subsequent service.

3 Experimental Method

3.1 Test Units

The test unit configuration shown in Fig. 2 was employed in this study to analyze the composite behavior of the proposed construction joint. The test unit was 4.13 m long, 1.8 m wide, and 3.35 m high. The length of the steel girder segment was set to 2.745 m from the steel support, more than four times its depth, to realize flexural behavior at the joint. The construction joint was installed between the steel girder and pier after the steel girder was fixed using four anchors. A 2.2-m-long and 1.8-m-wide concrete foundation was first constructed at the bottom of the pier to fix the test unit before tying the steel reinforcing bars and casting the pier on top. The compressive strength of the concrete, which is the average of five specimens according to ACI 311.6-18 (2018), was 45 MPa in the foundation, 35 MPa in the pier, and 40 MPa in the construction joint. In addition, four 24-mm-diameter chemical anchors with a yield strength of 450 MPa were used to connect the girders to the pier. The steel reinforcement was grade 60, as suggested by ASTM A615/A615M (2016). Grade 60 steel was also used for the steel girders, as suggested by ASTM A572/A572M (2015).

In this study, the uses of the construction joint and anchors were set as the experimental parameters, and three test units for Joints A, B, and C were designed accordingly (Table 1). Joint A reflected a typical joint in a composite rigid-frame bridge, in which the steel girder was fixed to the assembled steel reinforcement on the pier before the concrete was poured. Joint B employed a steel support to share the girder load and a construction joint to connect the steel girder to the concrete pier. Joint C was the same as Joint B, except the steel girder was also fixed to the concrete pier using anchors prior to casting the joint.

Fig. 3 shows the test unit construction process. The steel reinforcement cage of the foundation was first assembled (Fig. 3a), formwork was erected, and concrete was poured (Fig. 3b). After the foundation was cured for 14 days, the steel reinforcement for the pier was assembled as shown in Fig. 3c. For the Joint A test unit, which did not include a construction joint, the steel girder was then installed atop the assembled steel reinforcement cage of the pier, then the pier concrete was poured and cured for 14 days. For the Joint B and C test units, the pier formwork was erected around the tied cages, including block-outs and additional steel reinforcement for the construction joint, then the pier concrete was poured (Fig. 3d). After the pier concrete was cured for 14 days, the steel girder was mounted on the top surface of each pier and, in the case of Joint C, fixed to the pier by the anchors, as shown in Fig. 3e. Concrete was subsequently poured into the joints and cured for 28 days (Fig. 3f).

Fig. 4 illustrates the construction process for the chemical anchors. In total, four M24 chemical anchors were applied, consisting of two outer anchors and two inner anchors, each with a designed tensile strength of 41.5 kN. The process begins by drilling a hole into the concrete, as shown in Fig. 4a. Next, epoxy is injected and anchor bolts are inserted, which are then cured for four hours (Fig. 4b). Once the anchor bolts are fixed to the concrete, the steel and anchor bolts are connected, as depicted in Fig. 4c. Finally, Fig. 4d shows a photograph of the resulting connection between the steel frame and the concrete.

3.2 Test Procedures

Fig. 5 shows the set-up employed to conduct the load tests in this study, primarily comprising a steel frame with sufficient stiffness to apply a vertical load using a universal testing machine actuator with a capacity of 1000 kN. To ensure flexural behavior at the joint, the actuator was placed 280 mm from the far end of the steel girder. The height of the steel girder and distance from the loaded position were 0.55 and 2.465 m, respectively. As the length-to-height ratio exceeded 4, a flexural failure occurred because of the domination of bending

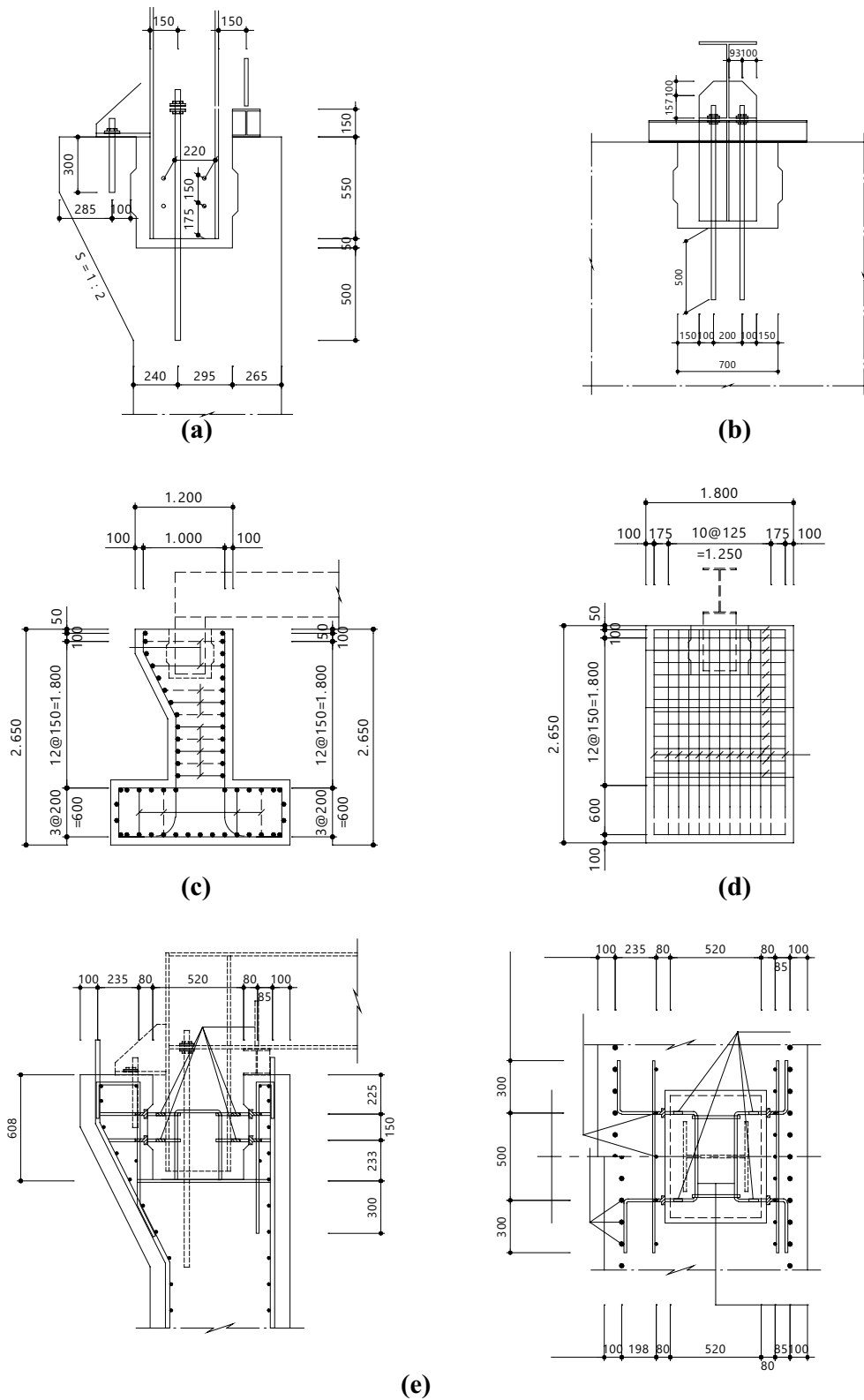
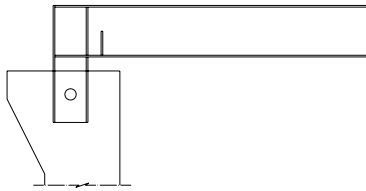
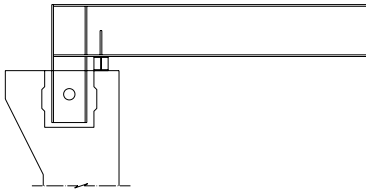
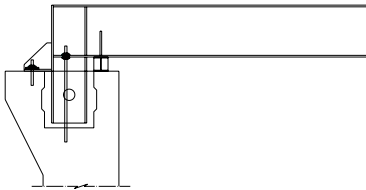


Fig. 2 Proposed construction joint with anchors: **a** side view, **b** front view, **c** side steel reinforcement view, **d** front steel reinforcement view, and **e** additional steel reinforcement

Table 1 Experimental parameters

Joint type	Schematic	Cast-in-place concrete joint	Anchors
A		No	No
B		Yes	No
C		Yes	Yes

behavior. Displacement was measured at the point of load application using a 200 mm linear variable differential transducer and the strain was measured by installing strain gauges on the steel girder, anchor, and steel reinforcement, as shown in Fig. 5a. Displacement control was adopted to apply the load at a rate of 0.03 mm/s up to a deflection of 30 mm in the vertical direction, after which the displacement rate was increased to 0.1 mm/s. The vertical position of the actuator was ensured by the actuator swivel-head mounting arrangement on the wheel spindle. The boundary conditions of the test units were set using several steel bars installed through the foundation on the front and back sides, as shown in Fig. 5b.

4 Experimental Results

Fig. 6 shows the vertical displacement results measured 280 mm from the end of the steel girder according to joint type. For Joints A and B, cracks developed at the interface between the steel girder and concrete at a load of 50 kN, whereas for Joint C, cracks did not develop until a load of 100 kN was applied. Fracture occurred at the interface between the steel girder and concrete at a load of 175 kN for Joints A and B, and at a load of 200 kN for Joint C. Thus, both interface cracking and fracture were clearly delayed owing to the anchors provided in Joint C. The ultimate capacity of Joint A was lowest at 240.6 kN, the ultimate capacity of Joint B was 16.5% higher at 280.2 kN, and Joint C exhibited the largest ultimate capacity at 353.2 kN, 46.8% higher than that of Joint A. Interestingly,

though Joint B exhibited a larger ultimate capacity than Joint A, it was accompanied by a smaller deflection. The ultimate capacity of Joint B therefore likely increased owing to the additional steel reinforcement provided in the construction joint.

Fig. 7 shows the strains in the outer and inner anchors of Joint C, 100 mm below the pier top, according to the applied load. The outer anchor exhibited only a small change in strain up to a load of 225 kN, above which the strain increased sharply. As the anchor used in this study was 24 mm in diameter and had a yield strength of 450 MPa, it was predicted that the anchor would yield at 2250 $\mu\epsilon$. Therefore, the outer anchor was estimated to have yielded when the load reached 330 kN, and a tensile strain of 3085 $\mu\epsilon$ occurred at a load of 353.2 kN. The inner anchor exhibited a small strain up to a load of 150 kN, then increased as the outer anchor yielded at a load of 225 kN. The strain in the inner anchor was 1604 $\mu\epsilon$ at a load of 353.2 kN. These results indicate that Joint C exhibited the largest elasticity and ultimate capacity owing to the strengthening effect of the anchors on the construction joint.

Fig. 8a shows the strain in the steel girder on the back stiffener, 350 mm below the top flange (where the back bracket was attached) according to joint type. Joint A exhibited nonlinear behavior owing to the fracture of the interface between the steel girder and concrete at a load of 175 kN. The strain in the steel beam for Joint B was smaller than that for Joint A because a smaller load was



(a)



(b)



(c)



(d)



(e)



(f)

Fig. 3 Test unit fabrication process: **a** assembling the steel reinforcement of the foundation, **b** fabrication of foundation formwork and pouring concrete, **c** assembling the steel reinforcement of the pier, **d** assembling the pier formwork and pouring concrete, **e** fixing the steel girder to the pier, and **f** pouring the concrete for the construction joint

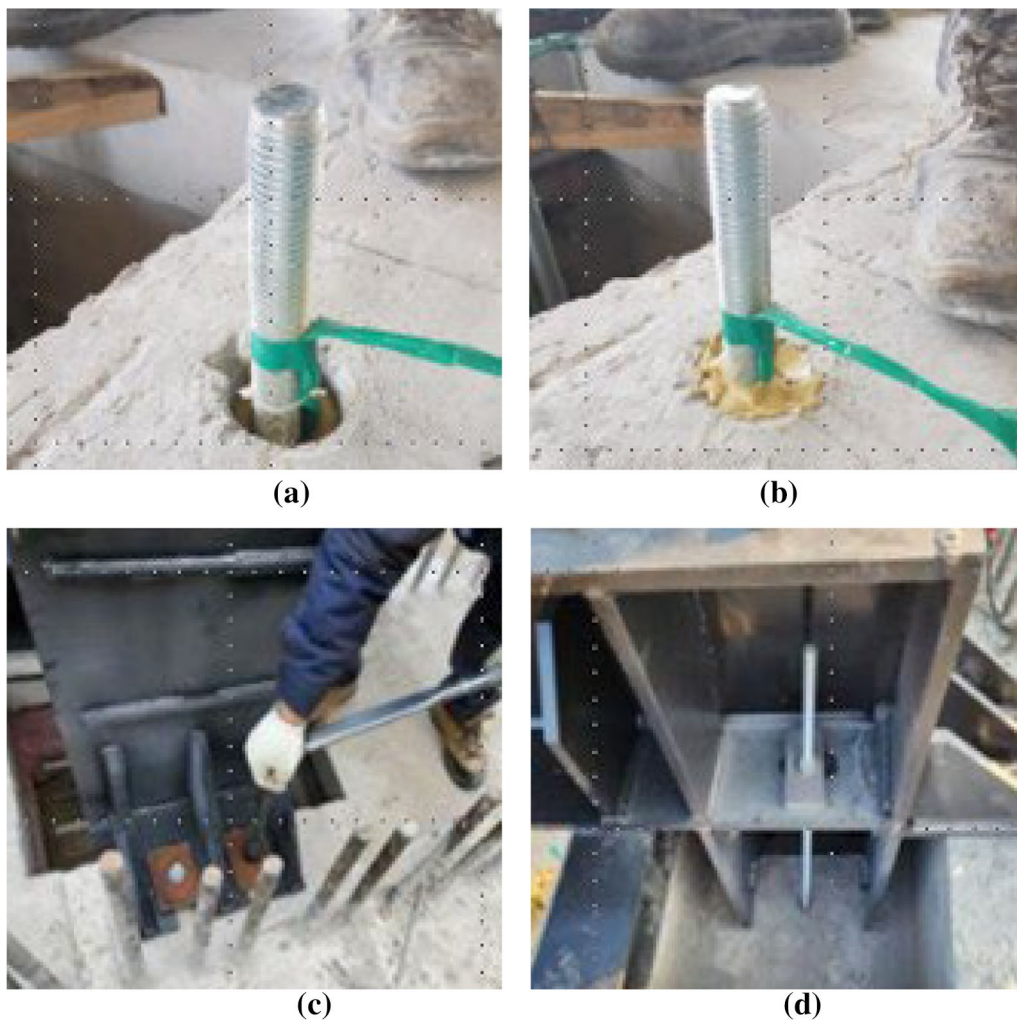
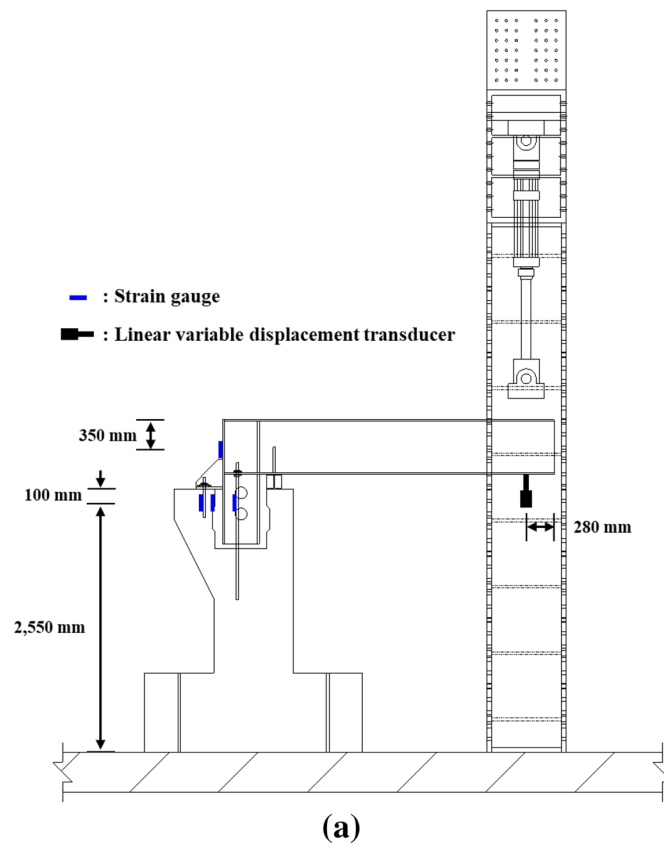


Fig. 4 Chemical anchor construction process: **a** hole drilling and anchor bolt insertion, **b** epoxy injection and curing, **c** inserting steel and fastening anchor bolts, **d** connection of steel girder and pier

applied to the steel girder at the same deflection owing to slippage between the construction joint and pier. Joint C exhibited the smallest strain at the same load because no slip occurred between the concrete casting joint and pier and the elasticity was improved, both owing to the presence of the anchors. The strain in the steel reinforcement, located 100 mm below the top of the pier and matching the elevation of the strain gauges on the anchors, varies depending on the joint type. Joints A, B, and C behaved similarly up to a load of approximately 200 kN; above this load, the strain behaviors in the steel reinforcement of the different piers diverged owing to the fracture at the interface between the steel girder and concrete. Thus, above a load of 200 kN, the strain in Joint A did not increase, the strain in Joint B exhibited rapid nonlinear behavior, and the strain in Joint C increased slowly owing to the secure anchor connection between components across

the concrete casting joint. Therefore, the steel girder, construction joint, and pier behaved compositely when using Joint C, providing the best structural performance.

Fig. 9 illustrates the crack patterns observed in the pier surfaces according to the joint type. Fig. 10 shows the damages for each joint. In joint A, microcracks occurred between the steel girder and the concrete connection. For Joints B, the horizontal cracks on the side of the pier were small owing to non-composite behavior between the steel girder and concrete. However, large vertical cracks formed where the steel girder met the rear end (span side) of the pier. For Joint B, a critical slip occurred between the construction joint and pier, causing cracks to appear between the steel girder and concrete. For Joint C, the steel girder and concrete acted together, no large horizontal cracks were observed on the sides of the pier, no vertical cracks were observed on the back of the pier,



(b)

Fig. 5 Test set-up: **a** loading and sensor arrangement, and **b** view of completed assembly

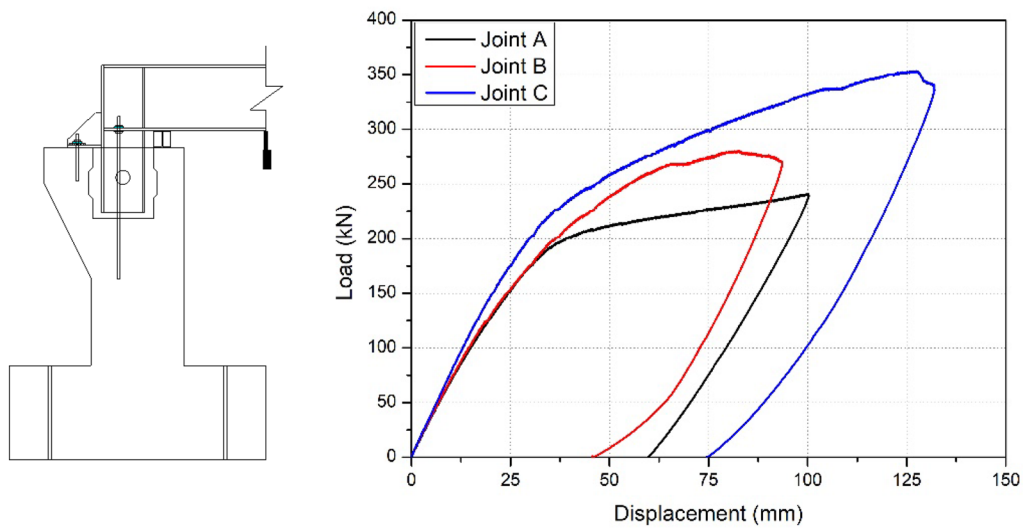


Fig. 6 Displacement results 280-mm from the beam end according to joint type

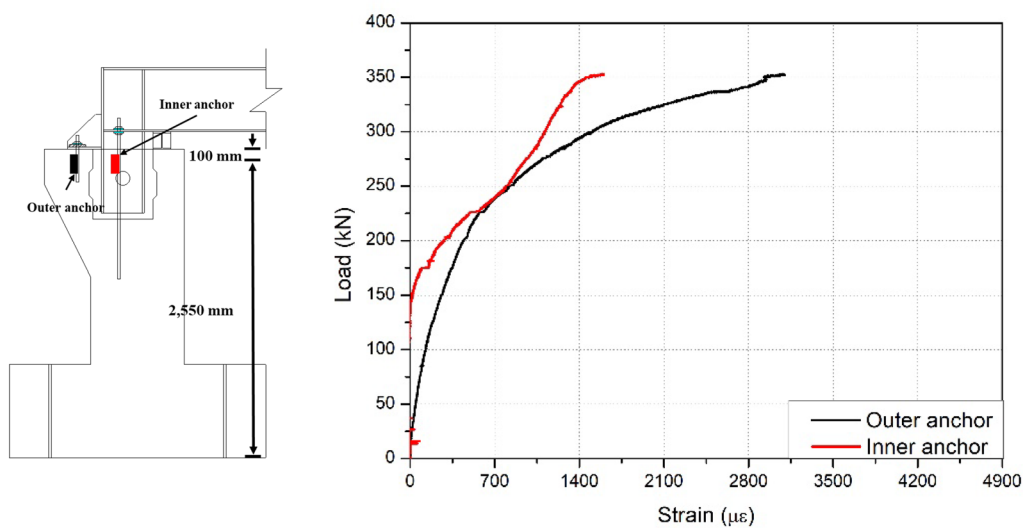


Fig. 7 Strain in the inner and outer anchors of Joint C

and no slip occurred between the concrete casting joint and pier. Thus, these results indicate that Joint C exhibited superior composite behavior.

5 Finite Element Model

5.1 Model Parameters

In this study, a three-dimensional (3D) finite element model of Joint C was constructed and verified against the measurements obtained during the corresponding experiment to analyze its structural behavior in detail. Various functions and finite elements provided in the ABAQUS software (Dassault, France) (2021) were used to construct the model and conduct the FEA. Fig. 11

shows the components and boundary conditions of the finite element model accordingly. The steel girder and steel support were modeled using quadrilateral shell elements with reduced integration (S4R) owing to their small thickness compared to their length. The concrete was modeled using the general-purpose linear brick element with reduced integration (C3D8R). The steel reinforcement was modeled using 3D Timoshenko beam (B31) elements to consider the shear strain in the construction joint and pier. Finally, the anchors and steel bars were modeled using 3D Euler–Bernoulli beam (B33) elements because they primarily experience longitudinal strain.

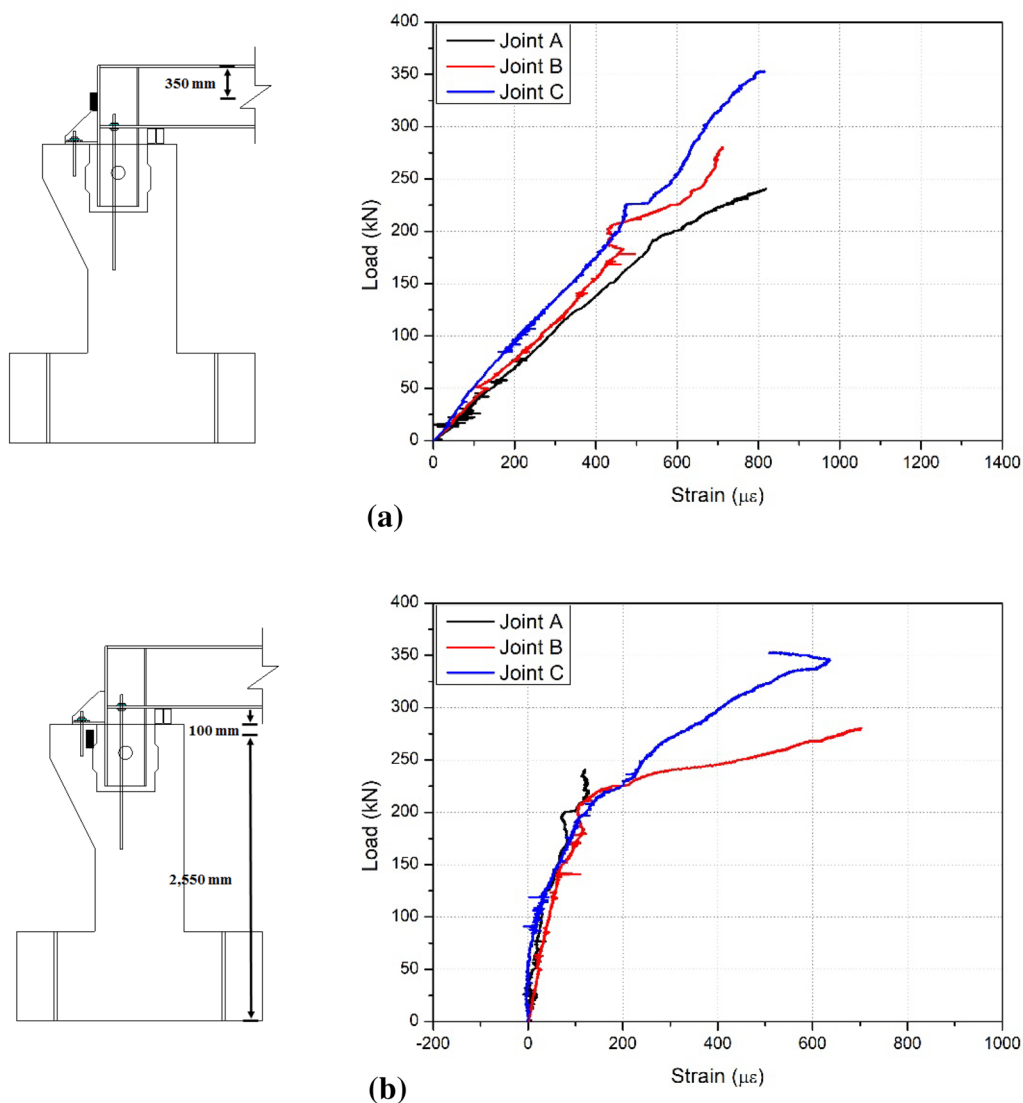


Fig. 8 Strain in the **a** steel girder back stiffener and **b** steel pier reinforcement according to joint type

When the plastic zone of each material was applied in the FEA, material nonlinearity was considered using a modeling technique provided in the Abaqus (2021) environment. The concrete damaged plasticity material model was employed to analyze the failure behavior of the concrete. However, the quantity of data generated by this model increases exponentially as it more accurately reflects the behavior of the actual material, imposing burdensome computational requirements. Therefore, this study simulated the plastic behavior of concrete by referring to the simplified concrete damaged plasticity material model suggested by Hafezolzghorani et al. (2017) to optimize the tradeoff between accuracy and computational resource requirements.

The Poisson’s ratio and elastic modulus of the concrete were set to 0.167 and 4700 MPa $\sqrt{f_c}$ (f_c = compressive strength of concrete), respectively, with reference to ACI 318-19 (2019). The tensile strength of concrete was evaluated as 10% of the compressive strength of concrete (Hafezolzghorani et al, 2017). The nonlinear material behaviors of the ductile materials, including the steel reinforcement, steel girder, steel support, and anchors, were simulated using the plastic material model provided in Abaqus (2021). Poisson’s ratio of 0.3 and elastic modulus of 200,000 MPa were used for the steel reinforcement, steel girder, steel support, and anchors, while their remaining material properties were defined according to ASTM A615/A615M (2016),

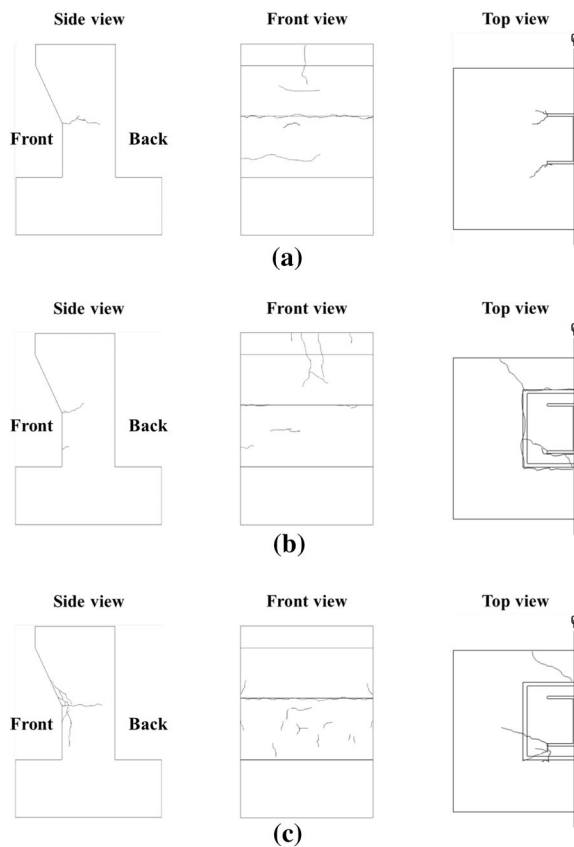
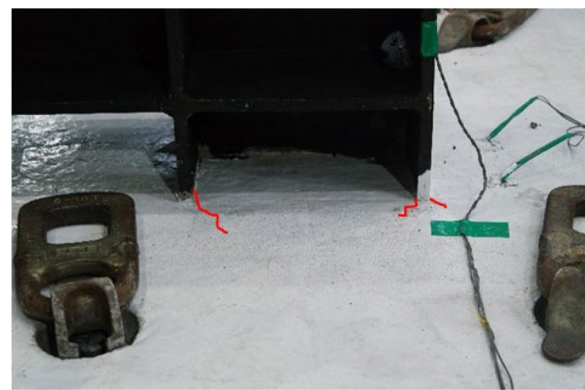


Fig. 9 Crack patterns in units for Joints **a**, **b**, and **c**

ASTM A572/A572M (2015), and ASTM E8/E8M (2011), respectively.

In this study, three interfaces were employed to model Joint C. The first interface was defined between the steel reinforcement and concrete. The embedded element technique provided by Abaqus (2021) was used to define the secondary elements embedded in the primary elements by constraining the degree of freedom in the rotation direction of the buried nodes. The embedded element technique has been frequently used to model tensile members embedded in structures such as steel reinforcement or anchors because it does not constrain the degree of freedom in the element rotation direction. The second interface was defined between the anchors and steel girder. Because the anchors were completely constrained by the steel girder, the multi-point constraint (MPC) available in Abaqus (2021) was used to integrate the behaviors of the primary and secondary nodes by attributing the degrees of freedom of the secondary (anchor) nodes to the primary (steel girder) nodes.

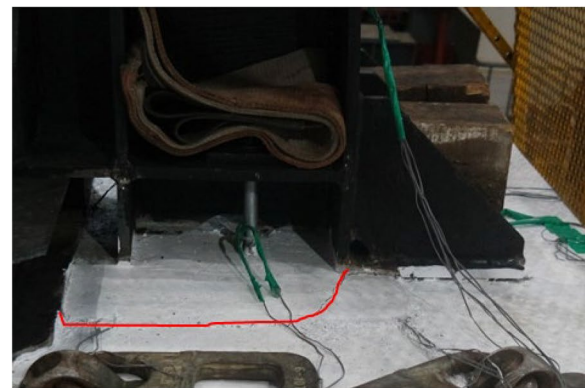
Fig. 11b shows the load and boundary conditions defined in the finite element model. A vertical, evenly distributed load was applied to the beam based on the



(a)



(b)



(c)

Fig. 10 Damage pictures in units for Joints **a**, **b**, and **c**

Newton–Raphson method. This load was increased in initial increments of 0.005, a minimum increment of 10^{-6} , and maximum increments of 0.005. Two types of boundary conditions were applied to the finite element model. First, in the experiment set-up employed in this study, the steel bars used to fix the pier foundation to the frame constrained the pier at fixed points; these constraints were applied to the model using the MPC to link the bottom end of each steel bar to the top of

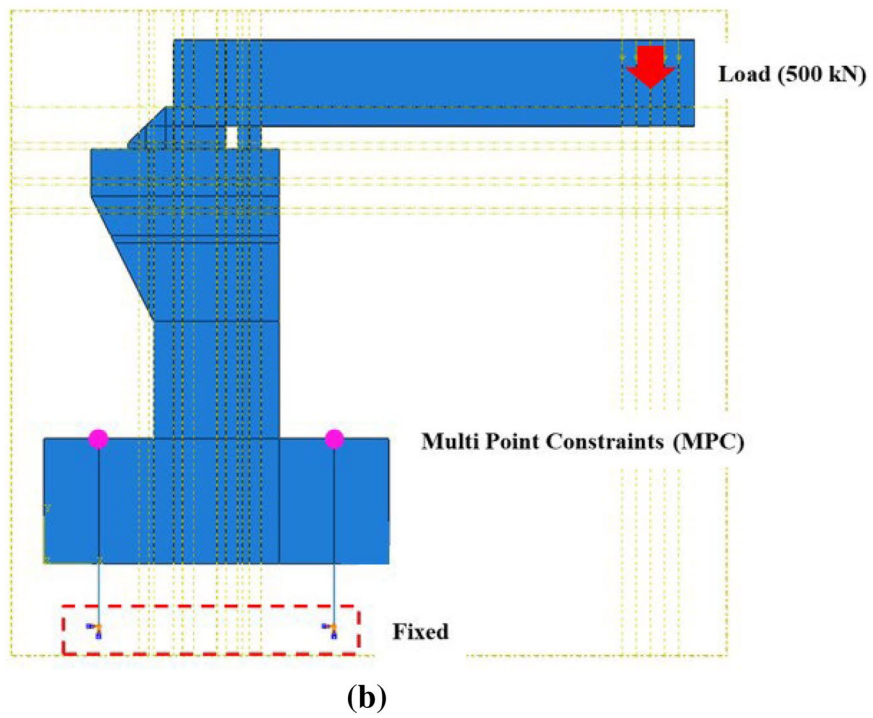
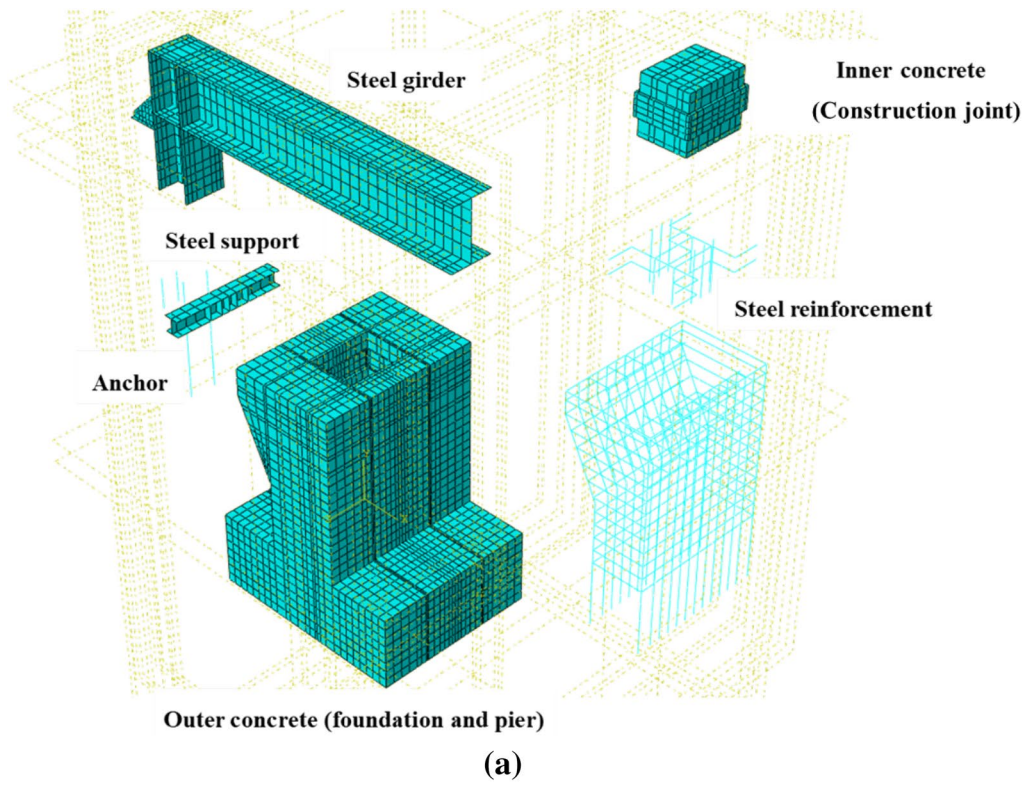


Fig. 11 Finite element model of Joint C: **a** mesh and **b** load and boundary conditions

the foundation. Second, because Joint C provided fixity between the pier and beam when the load was applied, the vertical strain was transferred to the inside edge of the base plate underlying the pier foundation.

5.2 Verification of Model

Fig. 12a shows the deflection 280 mm from the beam end owing to the load applied in the FEA. The experimental results for Joint C indicated that the initial cracking of the concrete occurred at a load of 100 kN, nonlinear behavior increased at a load of 200 kN, and the ultimate capacity was 353.2 kN. The FEA indicated initial cracking of the concrete at a load of 103 kN, an increase in nonlinear behavior at 205 kN, and a decrease in convergence as the load–deflection slope changed to negative at an ultimate capacity of 352.5 kN. Thus, the finite element model exhibited quite similar behavior to the test unit, with an error rate less than 3%.

Fig. 12b shows a comparison of the experimental and FEA-derived tensile strains according to the load applied to the steel girder. Both the test results and FEA exhibited nearly linear behaviors up to the ultimate capacity. The experimental strain at ultimate load was $833 \mu\epsilon$ and at the FEA-derived ultimate load was $798 \mu\epsilon$.

Fig. 12c, d compare the strains in the outer and inner anchors, respectively, according to the applied load in the experiment and FEA. The outer anchor (Fig. 10c) exhibited a higher strain in the finite element model ($4124 \mu\epsilon$) than in the experimental results ($3085 \mu\epsilon$), whereas the inner anchor (Fig. 11d) exhibited a lower strain in the FEA results ($1215 \mu\epsilon$) than in the experimental results ($1604 \mu\epsilon$). The outer anchor strain was larger in the FEA results because the connectivity between the anchor and concrete was ideally implemented in the finite element model; the strain in the inner anchor was smaller in the FEA because the outer anchor carried most of the load under ideal conditions.

Fig. 13 shows the maximum principal stress distributions in the pier according to the load applied in the FEA. The maximum principal stress distribution of the finite element analysis is the result of the front view. No stresses in the pier exceeded the tensile limit (3.5 MPa) up to a load of 150 kN. A notable region exceeding the tensile limit stress appeared in the side of the pier at a load of 200 kN. At higher loads, the concrete increasingly exceeded the tensile limit stress throughout the pier up to the ultimate load (353.5 kN), and the top side of the pier exceeded the tensile limit stress immediately before fracture. This maximum principal stress distribution was determined to be similar to the crack

pattern observed in the pier for Joint C. Consequently, the finite element model constructed in this study was considered to accurately predict the failure mode of the construction joint with anchors.

6 Parametric Study

In the proposed construction joint, the steel girder was installed and fixed to the concrete pier using anchors. Therefore, the structural performance of Joint C relies on the properties of the steel girder and anchors. However, the steel girder and anchors cannot be easily modified post-design because they are installed on-site after being prefabricated in a factory. Hence, the structural performance of the construction joint needs to be designed beforehand according to the properties of the steel girder and anchors. Therefore, the present study analyzed the structural performance of Joint C using the yield stress of the steel girder and nominal anchor diameter as the analysis parameters, as defined by the configurations shown in Table 2. In Group A, the yield stress of steel girder was increased from 290 (GR42) to 450 MPa (GR65) according to the intervening grades (GRs) presented in ASTM A572/A572M (2015). In Group B, the nominal anchor diameter was increased from 6 to 30 mm in increments of 6 mm, based on the anchors used in the test.

Fig. 14a shows the ultimate capacities of Joint C according to the yield stress of the steel girder (Group A). The ultimate capacity of the joint was 248.8 kN when GR42 steel with a yield stress of 290 MPa was used and increased linearly with increasing grade up to 382.4 kN for GR65. The ultimate capacities of GR55-ND24, GR50-ND24, and GR42-ND24 were lower than that obtained using the GR60 steel applied in the experiment (GR60-ND24) by 8.1%, 16.8%, and 29.4%, respectively, whereas that of GR65-ND24 was 8.5% higher. Thus, the structural performance of the joint can be predicted using the yield stress of the steel girder.

Fig. 14b shows the ultimate capacities of Joint C according to the nominal anchor diameter (Group B). The ultimate capacity consistently increased with anchor diameter from 292.5 kN for GR60-ND06 to 380.0 kN for GR60-ND30. In fact, the results of the FEA indicated that a clear correlation existed between the nominal anchor diameter and the ultimate capacity of the joint. Based on this correlation, the ultimate capacity of a construction joint with no anchors (nominal anchor diameter = 0 mm) was predicted to be 281.2 kN, which is within 0.5% of the ultimate capacity of 280.2 kN obtained by the Joint B experiment. Therefore, these

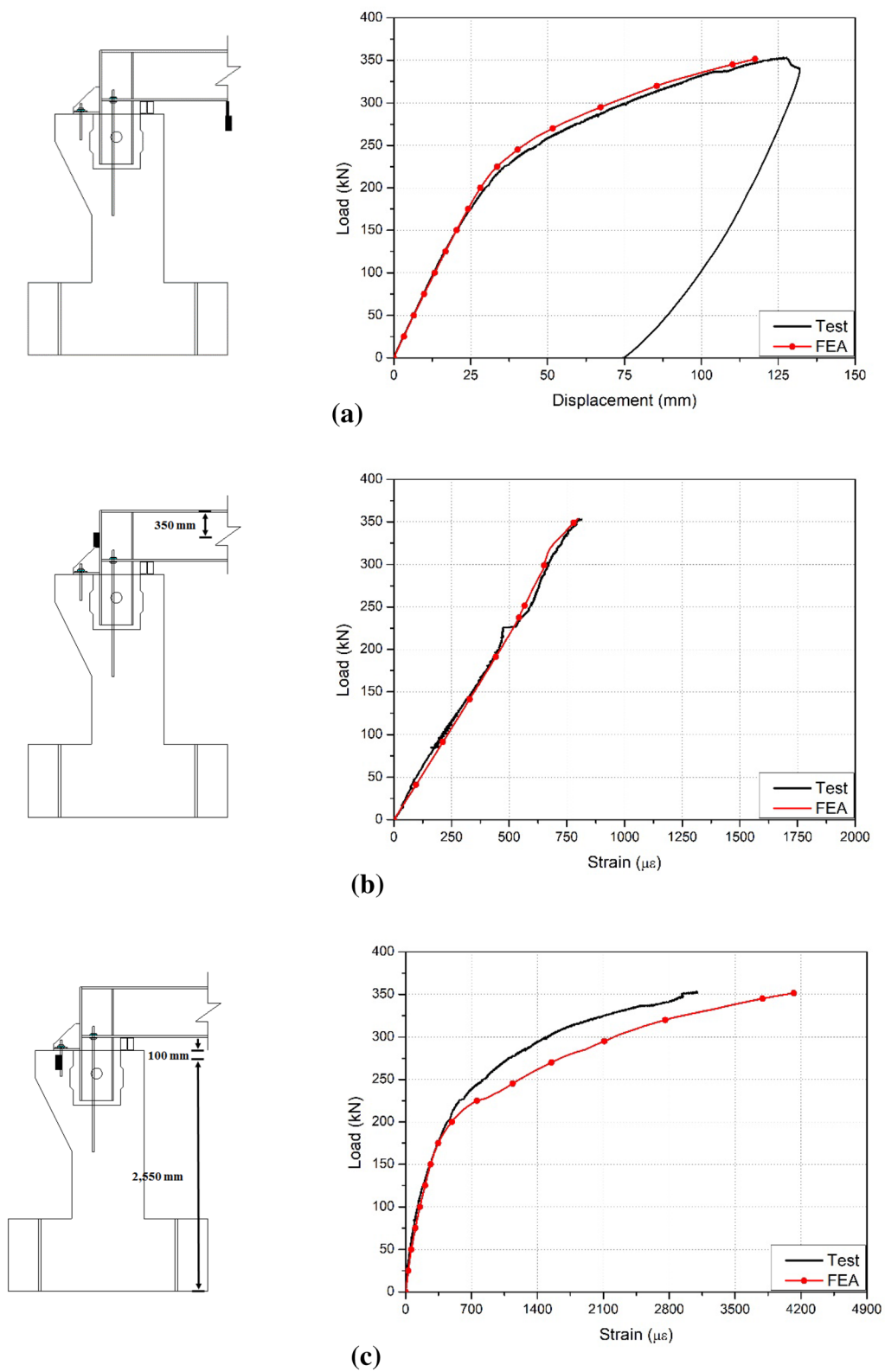


Fig. 12 Comparison of load–deformation/strain curves obtained by FEA and tests of Joint C at **a** 280 mm from the beam end, **b** steel girder back stiffener, **c** outer anchor, and **d** inner anchor

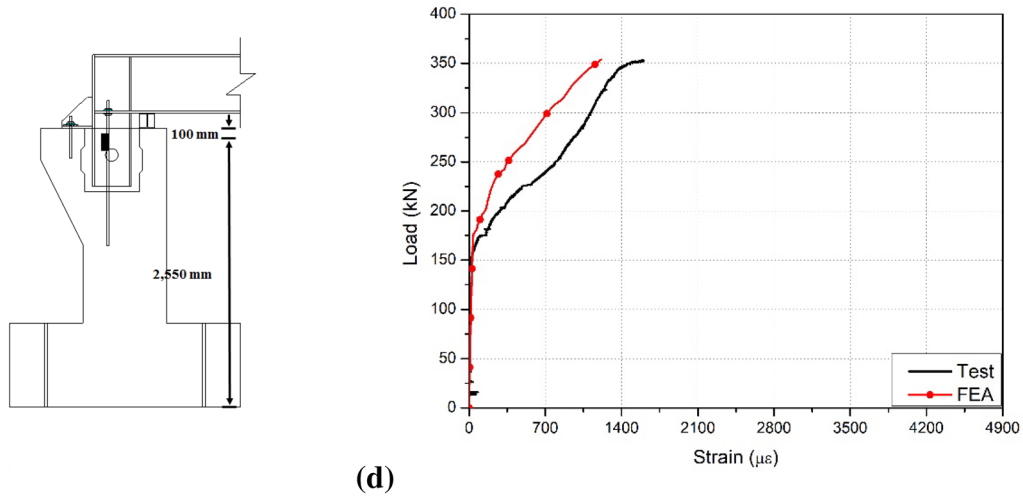


Fig. 12 continued

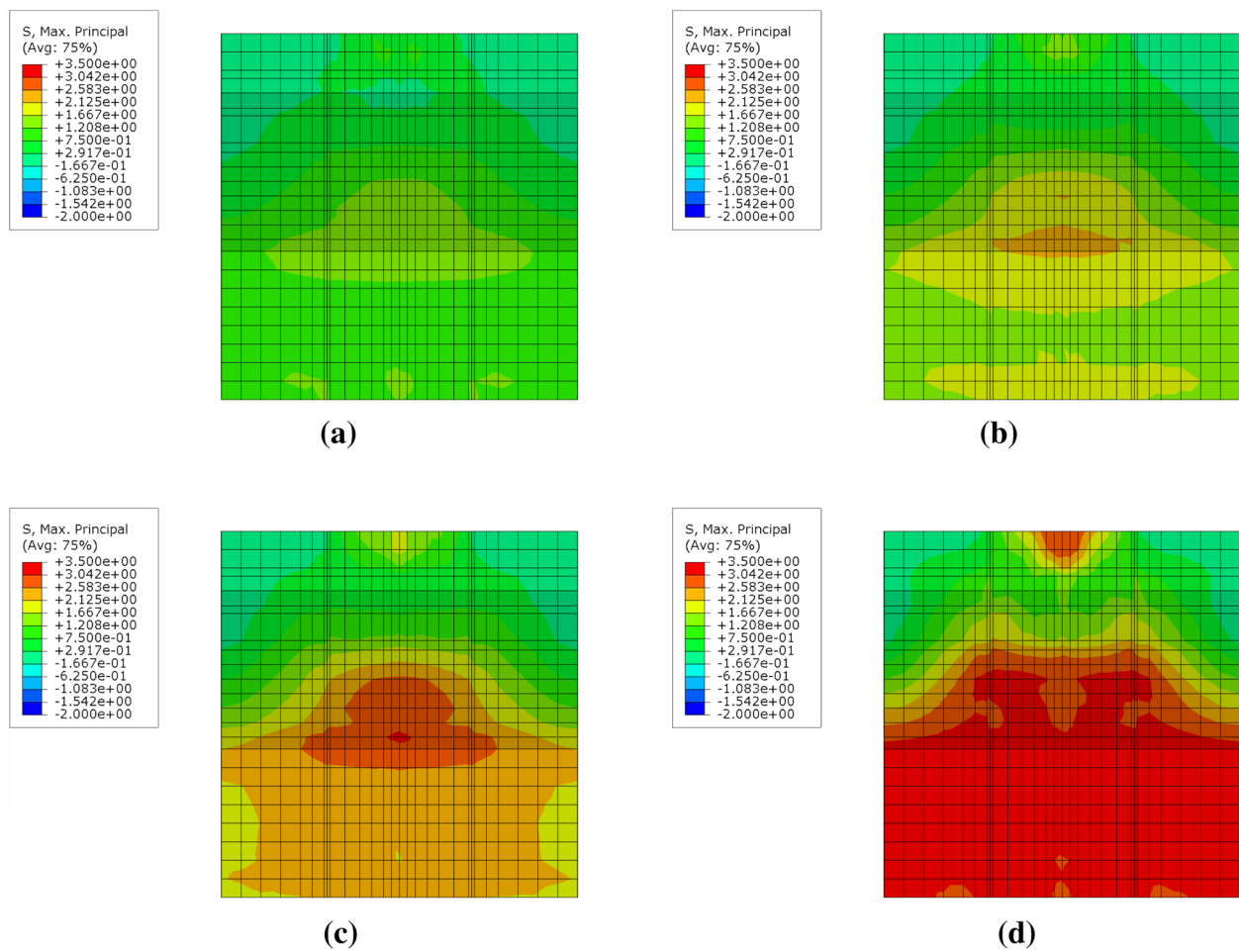


Fig. 13 Stress distributions in the finite element model of the Joint C pier at a load of **a** 100 kN, **b** 150 kN, **c** 200 kN, and **d** 352.5 kN (ultimate load)

Table 2 Parameters of the parametric FEA of Joint C

Group	Configuration	Yield stress in steel girder (MPa)	Nominal anchor diameter (mm)
Group A	GR42-ND24	290 (GR42)	24 (ND24)
	GR50-ND24	345 (GR50)	24 (ND24)
	GR55-ND24	380 (GR55)	24 (ND24)
	GR60-ND24	415 (GR60)	24 (ND24)
	GR65-ND24	450 (GR65)	24 (ND24)
Group B	GR60-ND06	415 (GR60)	6 (ND06)
	GR60-ND18	415 (GR60)	12 (ND12)
	GR60-ND24	415 (GR60)	18 (ND18)
	GR60-ND30	415 (GR60)	24 (ND24)
	GR60-ND30	415 (GR60)	30 (ND30)

results demonstrate that the ultimate capacity of the proposed construction joint with anchors can be predicted according to the nominal anchor diameter using the determined correlation.

7 Conclusions

In this study, three 3.35 m-high test units were fabricated to analyze the behaviors of different connections between the steel girder and concrete pier of a proposed composite rigid-frame bridge. Three joint types were evaluated: a direct connection between the steel girder and pier prior to pouring concrete (Joint A), a construction joint installed after casting the pier concrete and erecting the steel beam (Joint B), and a modification of Joint B using anchors to connect the steel beam directly to the concrete pier through the construction joint (Joint C). Load tests were then conducted to analyze the composite

behavior and structural performance of the three joint types. The structural performance of the Joint C was then further explored using an FEA verified against the experimental results to determine the relationship between steel girder yield stress, anchor diameter, and joint capacity. The conclusions of this study are as follows:

1. Joint B exhibited an ultimate capacity 16.5% larger than that of Joint A, but its corresponding displacement was smaller. Furthermore, intensive cracking was observed in Joint B, whereas cracking was relatively evenly distributed in Joint A. Consequently, composite behavior can be expected from Joint B owing to steel reinforcement interconnecting the construction joint and the pier. However, this composite behavior eventually decreased because of slip-page at the interface between the construction joint and pier.
2. Joint C provided the best structural performance among the three evaluated joint types in terms of stiffness, ultimate capacity, and behavior. Indeed, Joint C exhibited a higher stiffness than Joints A and B owing to the application of anchors with the construction joint, showing an ultimate capacity 46.8% greater than that of Joint A. Furthermore, Joint C exhibited superior composite behavior than did Joint B because the anchors between the steel girder and the pier provided additional connectivity. The use of Joint C can therefore provide a composite rigid-frame bridge that exhibits excellent integrity, composite behavior, and structural performance.

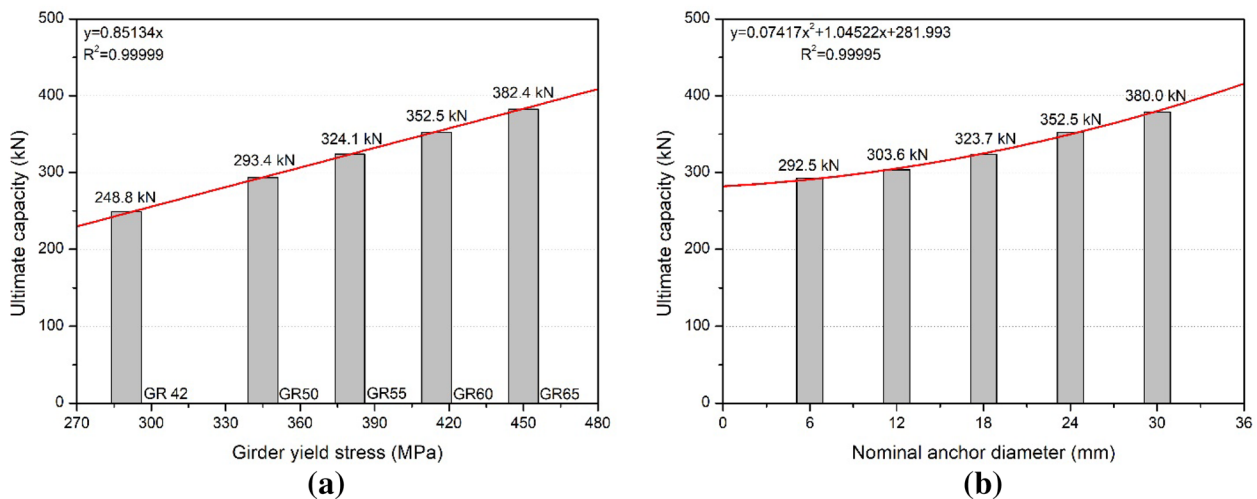


Fig. 14 Ultimate capacities of Joint C determined by the parametric study according to the **a** yield stress of the steel girder and **b** nominal anchor diameter

3. The FEA conducted in this study indicated similar behaviors to those observed during the Joint C experiments, with an error rate less than 3%. Indeed, similar strains were obtained in the steel girder and anchors by the Joint C experiment and FEA, and the stress distribution obtained by the FEA was similar to the crack pattern observed in the Joint C experiments. Thus, the finite element model was considered to accurately predict the behavior and failure mode of the proposed construction joint with anchors.
4. A parametric study was conducted to determine the effects of the yield stress of the steel girder and the nominal anchor diameter on the ultimate capacity of the construction joint with anchors. As both the yield stress of steel girder and the nominal anchor diameter were found to exhibit a predictable correlation with the ultimate capacity of the joint, they are considered to be the primary considerations in the joint design and behavior prediction.
5. The proposed construction joint with anchors can therefore be confidently designed and deployed for use in composite rigid-frame bridges to provide improved clearance, reliable composite behavior, rapid construction, and reduced maintenance costs.

Acknowledgements

No applicable.

Author Contributions

SC: Writing-Original draft preparation, Conceptualization, Formal analysis; JC: Data curation, Investigation; HL: Formal analysis, Writing-Reviewing and Editing; WC: Writing-Reviewing and Editing, Project administration. All authors read and approved the final manuscript.

Funding

This research was supported by the Basic Science Research Program through the National Research Foundation of Korea (NRF) funded by the Ministry of Education (2020R1C1C1005448, 2021R1A2C1011517).

Availability of Data and Materials

The data and materials are included in the manuscript.

Declarations

Ethics Approval and Consent to Participate

Not applicable.

Consent for Publication

Not applicable.

Competing Interests

The authors declare that they have no competing interests.

Received: 14 November 2022 Accepted: 18 May 2023

Published online: 23 October 2023

References

- Abaqus 2021. (2021). *Providence (RI): Dassault systems simulia corp.*
- ACI 311.6-18. (2018). *Specification for testing ready-mixed concrete.* Farmington Hills (MI): American Concrete Institute.
- ACI 318-19. (2019). *Building code requirements for structural concrete.* Farmington Hills (MI): American Concrete Institute.
- Adeli, H., & Zhang, J. (1995). Fully nonlinear analysis of composite girder cable-stayed bridges. *Computers and Structures*, 54(2), 267–277.
- ASTM A572/A572M. (2015). *Standard specification for high-strength low-alloy columbium-vanadium structural steel.* West Conshohocken (PA): ASTM International.
- ASTM A615/A615M. (2016). *Standard specification for deformed and plain carbon-steel bar for concrete reinforcement.* West Conshohocken (PA): ASTM International.
- ASTM E8/E8M. (2011). *Standard test methods for tension testing of metallic materials.* West Conshohocken (PA): ASTM International.
- Ataei, A., Bradford, M. A., & Valipour, H. R. (2015). Experimental study of flush end plate beam-to-CFST column composite joints with deconstructable bolted shear connectors. *Engineering Structures*, 99, 616–630.
- Ataei, A., Zeynalian, M., & Yazdi, Y. (2019). Cyclic behaviour of bolted shear connectors in steel-concrete composite beams. *Engineering Structures*, 198, 109455.
- Chung, W., Jung, D., & Kim, S. M. (2013). Strength and behavior of a vertically pre-tensioned composite rigid frame bridge. *International Journal of Steel Structures*, 13(2), 367–378.
- Dicleli, M., Eng, P., & Albhaisi, S. M. (2003). Maximum length of integral bridges supported on steel H-piles driven in sand. *Engineering Structures*, 25(12), 1491–1504.
- Feng, P. C., Wu, Y. Y., Yang, Y. Q., & Li, C. Y. (2006). Analysis of accident of bursting crack in bottom slab of a continuous rigid-frame bridge. *World Bridges*, 1, 66–69.
- Hafezolzghorani, M., Hejazi, F., Vaghei, R., Jaafar, M. S. B., & Karimzade, K. (2017). Simplified damage plasticity model for concrete. *Structural Engineering International*, 27(1), 68–78.
- Kwak, H. G., & Seo, Y. J. (2000). Long-term behavior of composite girder bridges. *Computers and Structures*, 74(5), 583–599.
- Lee, H., Min, J., Cho, S., & Chung, W. (2019). Lateral loading performance of the joint between a precast concrete girder and a steel pier. *Engineering Structures*, 198, 109551.
- Lin, Y., Bi, K., Zong, Z., Hao, H., Lin, J., & Chen, Y. (2020c). Seismic performance of steel-concrete composite rigid-frame bridge: Shake table test and numerical simulation. *Journal of Bridge Engineering*, 25(7), 04020032.
- Lin, Y., Zong, Z., Bi, K., Hao, H., Lin, J., & Chen, Y. (2020a). Experimental and numerical studies of the seismic behavior of a steel-concrete composite rigid-frame bridge subjected to the surface rupture at a thrust fault. *Engineering Structures*, 205, 110105.
- Lin, Y., Zong, Z., Bi, K., Hao, H., Lin, J., & Chen, Y. (2020b). Numerical study of the seismic performance and damage mitigation of steel-concrete composite rigid-frame bridge subjected to across-fault ground motions. *Bulletin of Earthquake Engineering*, 18(15), 6687–6714.
- Mei, G. (1999). Stability analysis of the continuous rigid frame bridge with high pier and large span. *Journal of xi'an Highway University*, 3(7), 1.
- Nakai, Y., Ha, T. M., & Fukada, S. (2018). Structural behavior of reinforced concrete slab rigid-frame bridge with h-shaped steel girders. *International Journal of Steel Structures*, 18(4), 1219–1241.
- Nijgh, M. P., Girbacea, I. A., & Veljkovic, M. (2019). Elastic behaviour of a tapered steel-concrete composite beam optimized for reuse. *Engineering Structures*, 183, 366–374.
- Sritharan, S., Vander Werff, J., Abendroth, R. E., Wassef, W. G., & Greimann, L. F. (2005). Seismic behavior of a concrete/steel integral bridge pier system. *Journal of Structural Engineering*, 131(7), 1083–1094.
- Wolde-Tinsae, A. M., Klinger, J. E., & Mullangi, R. (1988). *Bridge deck joint rehabilitation or retrofitting.* Final report. Washington DC: Federal Highway Administration; 1988. Report No. FHWA/MD-89/12.
- Xiang, Y. Q., Yao, Y. D., Hu, F. Q., Jing, L. J., & Zhu, W. G. (2004). Study of static and dynamic behavior of T-shape rigid frame bridge reinforced by prestressed external tendon. *China Journal of Highway and Transport*, 1, 009.

- Xie, Y., Yang, H., Zuo, Z., Sirotiak, T. L., & Yang, M. (2018). Optimal steel section length of the composite rigid-frame bridge. *Practice Periodical on Structural Design and Construction*, 23(3), 05018001.
- Zhang, J., Ding, C., Rong, X., Yang, H., & Li, Y. (2020). Development and experimental investigation of hybrid precast concrete beam–column joints. *Engineering Structures*, 219, 110922.
- Zhang, Y., Chen, B., Liu, A., Pi, Y. L., Zhang, J., Wang, Y., & Zhong, L. (2019). Experimental study on shear behavior of high strength bolt connection in prefabricated steel–concrete composite beam. *Composites Part b: Engineering*, 159, 481–489.
- Zhouhong, Z., Canglin, L., Youqin, L., & Weixin, R. (2004). Analysis of dynamic characteristics of a large-span prestressed concrete continuous rigid frame bridge. *Earthquake Engineering and Engineering Vibration-Chinese Edition*, 28(3), 98–104.

Publisher's Note

Springer Nature remains neutral with regard to jurisdictional claims in published maps and institutional affiliations.

Sanghyeon Cho is Doctoral Candidate in Department of Civil Engineering, College of Engineering at Kyung Hee University, Gyeonggi, Republic of Korea.

Jungho Choi is Doctoral Candidate in Department of Civil Engineering, College of Engineering at Kyung Hee University, Gyeonggi, Republic of Korea.

Heeyoung Lee is Assistant Professor in Department of Civil Engineering at Chosun University, Gwangju, Republic of Korea.

Wonseok Chung is Professor in Department of Civil Engineering, College of Engineering at Kyung Hee University, Gyeonggi, Republic of Korea.

Submit your manuscript to a SpringerOpen[®] journal and benefit from:

- ▶ Convenient online submission
- ▶ Rigorous peer review
- ▶ Open access: articles freely available online
- ▶ High visibility within the field
- ▶ Retaining the copyright to your article

Submit your next manuscript at ► [springeropen.com](https://www.springeropen.com)
